Fuel Cell Analysis

DOI: 10.1002/anie.200705516

Direct Visualization of Oxygen Distribution in Operating Fuel Cells**

Junji Inukai, Kenji Miyatake, Kenji Takada, Masahiro Watanabe, Tsuyoshi Hyakutake, Hiroyuki Nishide, Yuzo Nagumo, Masayuki Watanabe, Makoto Aoki, and Hiroshi Takano*

Fuel cells are devices that produce electric power by means of the chemical reaction of oxygen and fuels more efficiently than current technologies, and they are expected to become a cleaner source of energy.[1–4] Despite considerable recent advances, especially in polymer electrolyte membrane fuel cells (PEMFCs), existing technology still has drawbacks, including kinetic limitations on the oxygen reduction reaction[5,6] and the instability of Pt catalysts and polymer membranes nearby, in particular during startup–shutdown cycles.[4,7–9] The chemical reactions are uneven throughout the reaction field and not well understood. A central issue in fuel cell research is the measurement of the parameters that determine performance during cell operation, a difficult task owing to the structure of these devices. The distribution of liquid water in operating fuel cells has been measured and imaged through neutron radiography,[10,11] by NMR spectroscopy,[12,13] and by X-ray microtomography,[14] and temperatures have been recorded with a thermograph.[15] Hydrogen cross-over from the anode to cathode has been studied by mass spectrometry and magnetic resonance imaging in an operating PEMFC.[16] Oxygen consumption and H_2O_2 formation, as well as the local catalytic activity of a catalyst have been investigated and visualized in solution with a scanning electrochemical microscope.[17] However, to improve the performance and durability of PEMFCs,[18–20] it is crucial to understand distributions in real time not only of liquid water but also of reactants and products (oxygen, fuel, CO_2, water vapor, etc.) throughout the cell. Here we present a laboratory-use, nondestructive system for visualizing oxygen distribution in the interior of the operating fuel cells which relies on dye films[21,22] painted on the transparent gas flow field. Oxygen partial pressures were successfully visualized with spatial and time resolutions of 300 μm and 500 ms, respectively. We found that the oxygen distribution in PEMFC is not in accordance with that expected based on the current, which suggests a significant contribution from water. This imaging system is applicable to other important parameters such as water, carbon monoxide, and temperature, and should help in the design of new fuel cell separators and a reaction field called a membrane-electrode assembly (MEA).

An oxygen-sensitive porphyrin, tetrakis(pentafluorophenyl)porphyrinatoplatinum (PtTFPP), was used in the visualization system. This dye complex was dispersed in an oxygen-permeable polymer matrix, poly(1-trimethylsilyl-1-propyne) (pTMSP),[22,23] for making a thin, water-insoluble dye film. To understand the properties of the dye film, we placed the film in an environment with controlled oxygen partial pressure (mixtures of oxygen, nitrogen, and water vapor at 0–26 kPa of a total of approximately 101.3 kPa), temperature, and humidity, and irradiated it with a laser light at a wavelength of 407 nm. The emission from the film was filtered (> 600 nm), and the intensity was measured with a charge-coupled device (CCD) camera. Figure 1 a shows a Stern–Volmer plot[24] of the dye film at 80 °C with different relative humidities (RHs) (0, 16, 42 %), where I_{ref} is the emission intensity at p_{ref}, or the oxygen partial pressure in air. A phosphorescence quenching by oxygen with negligible influence from the water vapor concentration is clearly evident. Figure 1 b shows the emission intensity as a function of the temperature. The change in the emission was very small, namely $-0.5\,\%\,K^{-1}$.

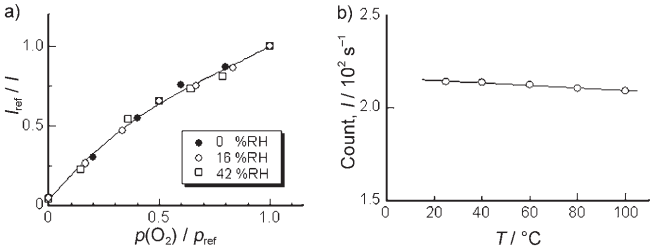

Figure 1. a) Stern–Volmer plots for gas mixtures (oxygen + nitrogen) with different relative humidities, %RH; cell temperature = 80 °C. The emission intensity, I, was measured for different oxygen partial pressures, $p(O_2)$. I_{ref} is the emission intensity at p_{ref}, or the oxygen partial pressure in air. b) Emission intensities in air at different temperatures.

[*] Prof. Dr. J. Inukai, Prof. Dr. K. Miyatake, K. Takada, Prof. Dr. M. Watanabe
Clean Energy Research Center
University of Yamanashi
4 Takeda, Kofu, Yamanashi 400-8510 (Japan)
Fax: (+81) 55-220-254-0371
E-mail: m-watanabe@yamanashi.ac.jp
T. Hyakutake, Prof. Dr. H. Nishide
Department of Applied Chemistry, Waseda University
3-4-1 Okubo, Shinjuku, Tokyo 169-8555 (Japan)
Y. Nagumo, M. Watanabe
Shimadzu
3-9-4 Hikaridai, Seika-cho, Kyoto 619-0237 (Japan)
Dr. M. Aoki, H. Takano
Fuji Electric AT
7 Yahatakaigan-dori, Ichihara, Chiba 290-8511 (Japan)

[**] This study was supported by the New Energy and Industrial Technology Development Organization (NEDO) (Japan). The authors thank Profs. A. Wieckowski, P. P. Edwards, D. J. Schiffrin, and T. Zawodzinski for their comments, Prof. D. A. Tryk for his help in writing the manuscript, and Y. Ishigami for his experimental help.

Supporting information for this article is available on the WWW under http://www.angewandte.org or from the author.

Figure 2a schematically shows the structure of the PEMFC for oxygen visualization. The dye film was coated on the oxygen channel of the separator (Figure 2b) or on a

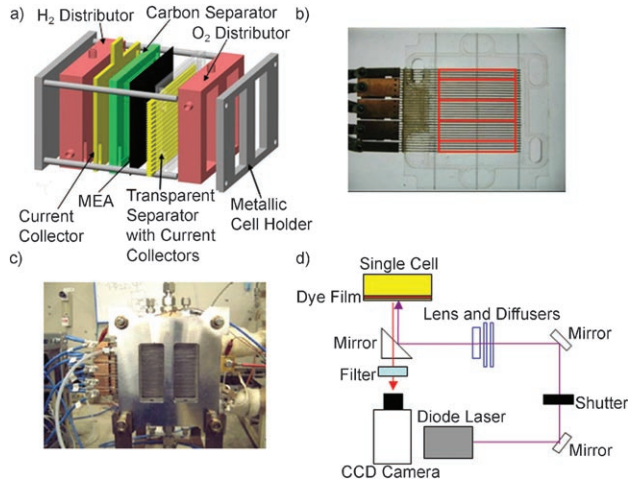

Figure 2. a) Schematic representation of the oxygen visualization cell. b) Transparent separator with current collectors of gold-plated metal ribs; imaging area = 10 × 10 cm; channel width = 2 mm; channel depth = 1 mm; rib width = 1 mm. Current collectors were separated into five sections (outlined in red). c) A PEMFC cell. d) Schematic diagram of the oxygen-imaging system using a dye film on transparent polyacrylate resin.

plate one centimeter thick fabricated specially of transparent polyacrylate resin. Current was collected by gold-plated stainless steel attached to the plate. These current collectors were designed to be separated into five sections in the cell, which made it possible to calculate the oxygen consumption at the end points of each section by measuring the currents, with the assumption that all the currents were produced from the reaction between oxygen and hydrogen in the cell. Figure 2c shows a photograph of the cell used in this study. During cell operation, excitation from a 407-nm laser was employed. The laser beam was diffused, spread, and distributed uniformly (50 $\mu W\,cm^{-2}$) onto the separator. The emission from the dye film through the transparent separator was filtered (> 600 nm), and images were captured with a CCD camera (1 pixel ≈ 0.2 mm). A schematic illustration of the phosphorescence imaging system for measuring the oxygen partial pressure in a PEMFC is shown in Figure 2d.

For quantitative analyses, the emission was obtained in advance using mixtures of oxygen and nitrogen at various oxygen partial pressures (0–26 kPa at a total of approximately 101.3 kPa) without current at a typical operating temperature of 70 °C and a relative humidity of 50 %. The oxygen partial pressure in the cell was cross-checked using an oxygen monitor. While the emission data was being recorded, the gas flow was stopped in order to avoid the generation of a pressure difference between the inlet and outlet. Figure S1 in the Supporting Information shows three emission images obtained for the calibration. It is clearly seen that the emission intensity from the dye film decreases as the oxygen partial pressure increases, although there is some nonuniformity owing to the nonuniformity of the irradiation. A calibration curve, Stern–Volmer plot, was obtained for each pixel from the emission at different oxygen partial pressures and was fitted with a cubic polynomial. Figure S2 in the Supporting Information shows examples of emission intensity curves and Stern–Volmer plots at 10 locations in a flow channel. All the data at a given $p(O_2)$ value for the different positions fit the same regression line regardless of the nonuniformity mentioned above. The Stern–Volmer plots recorded at 500 × 500 individual pixels in an image were thus taken into account for the precise measurement of the oxygen partial pressures throughout the flow channel with a spatial resolution of 0.2 mm.

While the cell was operating, humidified air (RH = 50 %) with an oxygen partial pressure of 18.0 kPa was brought in from the upper left and exhausted at the lower-right end of a winding channel (the middle of the cell was tightened by a cell-holder plate as shown in Figure 2a and c). The luminescent intensity of images was measured at each pixel during the actual operation and was subsequently converted to the oxygen partial pressure. Figure 3 shows steady-state images of

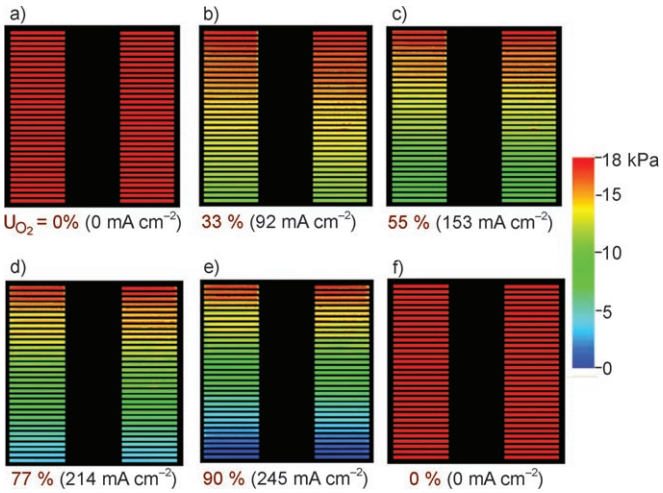

Figure 3. Oxygen partial pressures visualized in an operating PEMFC. Cell temperature = 70 °C; relative humidity = 50 % (air and H_2); air flow = 500 mL min^{-1}, H_2 flow = 500 mL min^{-1}, current density = 0 (a), 92 (b), 153 (c), 214 (d), 245 (e), and 0 mA cm^{-2} (f), oxygen utilization = 0 (a), 33 (b), 55 (c), 77 (d), 90 (e), and 0 % (f). 128 images were accumulated for each set of conditions.

oxygen partial pressures along the gas-flow channel in an operating fuel cell for overall oxygen utilizations (U_{O_2}) of 0, 33, 55, 77, and 90 % (0, 92, 153, 214, and 245 mA cm^{-2}, respectively). 128 images were successively accumulated, which took approximately 2 min, and they were subsequently averaged at each set of conditions. The error in the experiments was estimated to be ± 2 % by statistical analysis of the repeated runs. As the oxygen utilization was increased (i.e., by increasing current density; Figure 3a–e), the oxygen partial pressures clearly decreased, and, as shown in each frame of Figure 3, oxygen utilization also decreased gradually

from the entrance to the exit. When the current density was changed back to 0 mA cm^{-2} (open circuit) (Figure 3 f), the oxygen pressure throughout the cell returned to 18.0 kPa.

Figure 4 shows the changes in oxygen partial pressure along the channel at various current densities (J_G) and U_{O_2} values, which were obtained directly by the visualization

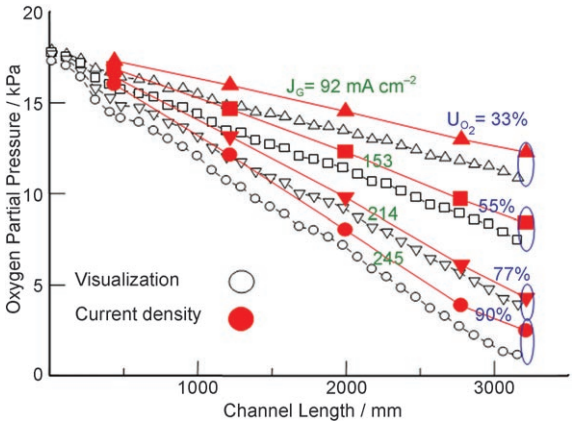

Figure 4. Oxygen partial pressures measured by visualization (open symbols) and calculated from the current density (filled red symbols) for a PEMFC.

method (white symbols) and by calculation from the sectional currents at the five current collectors (red symbols). The oxygen partial pressures decreased monotonically along the channel. The oxygen partial pressures calculated from the sectional currents are higher than those measured by our visualization method. In the calculation, the pressure along the channel was held at 101.3 kPa, which is equivalent to the inlet air pressure including the water generated as a cathode reaction product. However, the actual distribution of water and the rate of water transport into/out of the membrane (back diffusion and electroosmotic drag[25]) are unknown and not included in these calculations. Clearly, because of the influence of water vapor, the oxygen partial pressure calculated from the current is higher than that measured by our method. By analyzing this discrepancy, one can estimate the total effect of the water production, back diffusion, and osmotic drag at each point in the operating fuel cell. The water vapor pressure at each point must be visualized for the calculation, and we are now preparing for this experiment.

After the acquisition of steady-state images, we proceeded to transition imaging. Figure 5 shows the oxygen partial pressures at four selected points in the gas flow channel when the current density was increased to 61, 122, and 245 mA cm^{-2} for the simulation of startup–shutdown cycles. Images were obtained every 500 ms (see Movie S1 in the Supporting Information). At the open circuit, the oxygen partial pressure was slightly higher at measurement points closer to the entrance of the humidified air because of pressure drop along the channel. When the current density was changed, approximately 20 s was needed for the oxygen distribution throughout the cell to stabilize, even though the air was supplied at 500 mL min^{-1}, or 420 cm s^{-1} in the channel which was approximately 320 cm in length. This slow rate in the

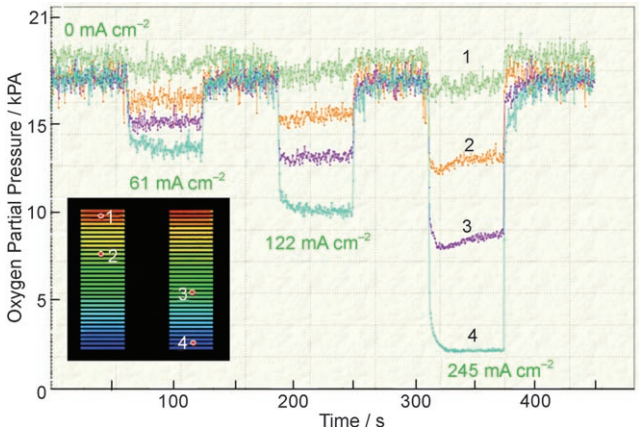

Figure 5. Oxygen partial pressures measured at four points (points 1–4) in a channel during the simulation of startup–shutdown cycles for a PEMFC. Current densities were stepped to 61, 122, and 245 mA cm^{-2}; oxygen utilizations were 22, 44, and 90%, respectively; measured area = 0.8 × 0.8 mm.

change in oxygen partial pressure, therefore, cannot be explained simply by the gas flow. During this 20 s, the oxygen partial pressures are seen to increase gradually after the initial pressure drop, at points 1, 2, and 3, whereas the pressure continued to decrease at point 4 (see Figure 5).

We have demonstrated that our new imaging system is a unique research tool for visualizing the oxygen partial pressures in a PEMFC and analyzing fuel cell performance. This system has already been applied to visualize oxygen partial pressures in a direct methanol fuel cell.[26] By combining other dye materials sensitive to temperature or CO_2 and infrared absorption for water vapor, we are now proceeding to the simultaneous visualization of these parameters to achieve even more accurate diagnoses of fuel cell performance.

Experimental Section

A solution of PtTFPP (commercial) and pTMSP (synthesized[22,23]) in toluene was spray-coated onto the air channel of the separator to form a dye film with a thickness of 2 μm and consisting of 10 wt% PtTFPP. The film was tested to be tolerant against water and high temperatures (100 °C). During the acquisition of Stern–Volmer plots, gas mixtures (oxygen + nitrogen + water vapor), prepared using mass flow controllers and a humidifier, were introduced in both the anode and cathode at atmospheric pressure. The oxygen partial pressure was also measured by an oxygen monitor at the inlet of the fuel cell. To reduce stray light, all reflecting materials of the cell were covered or painted black, and the laser light was operated in the dark. The Stern–Volmer plots were obtained at 500 × 500 pixels using a CCD camera, and the data were fitted at each pixel (0.2 × 0.2 mm^2) with a cubic polynomial. In this manner, 250000 calibration curves were obtained. During the cell operation, cell face was irradiated with the laser light, and the emission from a dye film coated on the air channel was captured by a CCD camera. Conversion from the emission to the oxygen partial pressure was carried out at each pixel by customized programs. In the calculation of the oxygen partial pressure from the sectional currents (Figure 5) at the five current collectors (Figure 2 b), we adopted 18.0 and 101.3 kPa for the oxygen partial pressure at the inlet and the total pressure along the channel,

respectively. The latter included oxygen, nitrogen, and water vapor. We also assumed that the total pressure along the channel was constant.

Received: December 3, 2007
Published online: March 5, 2008

Keywords: electrochemistry · fuel cells · luminescence · optical analysis · oxygen

[1] B. C. H. Steele, A. Heinzel, *Nature* **2001**, *414*, 345 – 352.
[2] C.-Y. Wang, *Chem. Rev.* **2004**, *104*, 4727 – 4766.
[3] *Catalysis and Electrocatalysis at Nanoparticle Surfaces* (Eds.: A. Wieckowski, E. Savinova, C. Vayenas), Marcel Dekker, New York, **2003**.
[4] *Advances in Fuel Cells*, *Vol. 1* (Eds.: K.-D. Kreuer, T. V. Nguyen, T. Zhao), Elsevier, Amsterdam, **2007**.
[5] V. R. Stamenkovic, B. S. Mun, M. Arenz, K. J. J. Mayrhofer, C. A. Lucas, G. Wang, P. N. Ross, N. M. Markovic, *Nat. Mater.* **2007**, *6*, 241 – 247.
[6] H. Yang, W. Vogel, C. Lamy, N. Alonso-Vante, *J. Phys. Chem. B* **2004**, *108*, 11024 – 11034.
[7] P. J. Ferreira, G. J. la O', Y. Shao-Horn, D. Morgan, R. Makharia, S. Kocha, H. A. Gasteiger, *J. Electrochem. Soc.* **2005**, *152*, A2256 – 2271.
[8] S. R. Samms, S. Wasmus, R. F. Savinell, *J. Electrochem. Soc.* **1996**, *143*, 1498 – 1504.
[9] F. Maillard, M. Eikerling, O. Cherstiouk, S. Schreier, E. Savinova, U. Stimming, *Faraday Discuss.* **2004**, *125*, 357 – 377.
[10] M. A. Hickner, N. P. Siegel, K. S. Chen, D. N. McBrayer, D. S. Hussey, D. L. Jacobson, M. Arif, *J. Electrochem. Soc.* **2006**, *153*, A902 – A908.
[11] Y.-S. Chen, H. Peng, D. S. Hussey, D. L. Jacobson, D. T. Tran, T. Abdel-Baset, M. Biernacki, *J. Power Sources* **2007**, *170*, 376 – 386.
[12] K. Teranishi, S. Tsushima, S. Hirai, *J. Electrochem. Soc.* **2006**, *153*, A664 – A668.
[13] K. W. Feindel, S. H. Bergens, R. E. Wasylishen, *Phys. Chem. Chem. Phys.* **2007**, *9*, 1850 – 1857.
[14] P. K. Sinha, P. P. Mukherjee, C.-Y. Wang, Chao-Yang, *J. Mater. Chem.* **2007**, *17*, 3089 – 3103.
[15] R. Shimoi, M. Masuda, K. Fushinobu, Y. Kozawa, K. Okazaki, *J. Energy Resour. Technol.* **2004**, *126*, 258 – 261.
[16] S. Tsushima, T. Nanjo, S. Hirai, *ECS Trans.* **2007**, *11*, 435 – 443.
[17] K. Eckhard, W. Schuhmann, *Electrochim. Acta* **2007**, *53*, 1164 – 1169.
[18] J. Zhang, K. Sasaki, E. Sutter, R. R. Adzic, *Science* **2007**, *315*, 220 – 222.
[19] V. R. Stamenkovic, B. Fowler, B. S. Mun, G. Wang, P. N. Ross, C. A. Lucas, N. M. Markovic, *Science* **2007**, *315*, 493 – 497.
[20] T. Yoda, H. Uchida, M. Watanabe, *Electrochim. Acta* **2007**, *52*, 5997 – 6005.
[21] *Pressure and Temperature Sensitive Paints* (T. Liu, J. P. Sullivan), Springer, Berlin, **2005**.
[22] K. Asai, Y. Amao, Y. Iijima, I, Okura, H. Nishide, *J. Thermophys. Heat Transfer* **2002**, *16*, 109 – 115.
[23] T. Masuda, E. Isobe, T. Higashimura, *J. Am. Chem. Soc.* **1983**, *105*, 7473 – 7474.
[24] Topics in *Fluorescence Spectroscopy*, *Vol. 2* (Ed.:J. R. Lakowicz), Springer, Berlin, **1991**.
[25] T. A. Zawodzinski, J. Davey, J. Valerio, S. Gottesfeld, *J. Electrochem. Soc.* **1996**, *143*, 1498 – 1504.
[26] J. Inukai, K. Miyatake, Y. Ishigami, M. Watanabe, T. Hyakutake, H. Nishide, Y. Nagumo, M. Watanabe, A. Tanaka, *Chem. Commun.* **2008**, DOI: 10.1039/B718692D.

